Time Dependent Driving Forces and the Kinetics of Tricalcium Silicate Hydration

Jeffrey W. Bullard[1]

National Institute of Standards and Technology, Gaithersburg, MD 20878, USA
Fax: +1-301990-6891; Tel: +1-301-975-5725; E-mail: jeffrey.bullard@nist.gov

George W. Scherer

Princeton University, Eng. Quad. E-319, Princeton, NJ 08544, USA
Fax: +1-609-258-2799; Tel: +1-609-258-5680; E-mail: scherer@princeton.edu

Jeffrey J. Thomas

Schlumberger-Doll Research, Cambridge, MA 02139, USA
Tel: +1-617-768-2196; E-mail: JThomas39@slb.com

Abstract

Simulations of tricalcium silicate (C_3S) hydration using a kinetic cellular automaton program, HydratiCA, indicate that the net rate depends both on C_3S dissolution and on hydration product growth. Neither process can be considered the sole rate-controlling step because the solution remains significantly undersaturated with respect to C_3S yet significantly supersaturated with respect to calcium silicate hydrate (C−S−H). The reaction rate peak is attributed to increasing coverage of C_3S by C−S−H, which reduces both the dissolution rate and the supersaturation of C−S−H. This supersaturation dependence is included in a generalized boundary nucleation and growth model to describe the kinetics without requiring significant impingement of products on separate cement grains. The latter point explains the observation that paste hydration rates are insensitive to water/cement ratio. The simulations indicate that the product layer on C_3S remains permeable; no transition to diffusion control is indicated, even long after the rate peak.

[1]Corresponding author.

Key words: hydration, modeling, nucleation, growth, supersaturation

1. Introduction

The transformation of a fluid slurry of cement particles into an elastic solid (a process known as "setting" of cement paste) involves the dissolution of the anhydrous cement and precipitation of the calcium silicate hydrate binder phase (called C−S−H[2]) onto the surfaces of the cement grains; setting corresponds to percolation of the overlapping product layers.

Dissolution of a solid, such as tricalcium silicate in water, is a net process consisting of one or more reaction paths leading to a final product of dissociated ions in solution. Each reaction path comprises multiple elementary reaction steps at the solid-liquid surface, although for tricalcium silicate the reaction paths and their elementary steps are, generally, poorly understood. Nevertheless, the overall driving force for dissolution is the free energy difference $\Delta\Phi_{\mathrm{d,net}}$ between the products of the final step (*i.e.*, the dissociated ions in solution) and the reactants of the first step (*i.e.*, the components in the solid); the net process will occur only if $\Delta\Phi_{\mathrm{d,net}} < 0$, which means that the solution is undersaturated with respect to the dissolving solid. Likewise, growth of a solid such as C−S−H is a net process that likely has one rate-controlling step among all the elementary steps leading from the reactant ions in solution to the final solid product, and that net process can occur only if $\Delta\Phi_{\mathrm{g,net}} < 0$, meaning that the solution is supersaturated with respect to the growing solid.

With this in mind, the overall phenomenon of cement hydration is a combination of at least two net processes that are coupled in series by virtue of the fact that the final products of cement dissolution are also the initial reactants needed for growth of hydration products. Because the two processes are linked in series, if either of them is near equilibrium then the other process controls

[2]Here we use cement chemistry notation, where C = CaO, S = SiO_2, H = H_2O; the hyphens in C−S−H indicate that it is not a stoichiometric compound.

the rate. For example, if the solution is close to equilibrium saturation with respect to the dissolving cement material, the overall rate of hydration will be controlled by the rate at which precipitation of C−S−H removes ions from the solution. During the course of the reaction, kinetic control could switch from one of these processes to the other, or a third process (such as transport through the precipitated layer of product) could take control.

In this paper, we investigate rate control during the hydration of tricalcium silicate (Ca_3SiO_5, abbreviated as C_3S), which constitutes about two-thirds of portland cement and is responsible for the setting and initial strengthing of cement paste [1]. To do this, we implement, using HydratiCA [2, 3], reasonable rate laws for C_3S dissolution [4] and for the nucleation and growth of C−S−H and of portlandite ($Ca(OH)_2$, abbreviated as CH) [3]. As described in the next section, HydratiCA evolves the system chemistry and 3D microstructure according to these rate laws, and it therefore enables one to track the consequences of the rate law assumptions for the time-dependence of solution composition and microstructure. The simulation results are used here to investigate the influences of the simultaneous rate processes on the net rate of hydration (*i.e.*, the overall rate as would be measured by isothermal calorimetry or chemical shrinkage measurements).

We also examine how mathematical models based on boundary nucleation and growth (BNG) [5, 6] are influenced by solution composition. These latter models are widely used to fit the kinetics of hydration [7–9] and typically assume that the growth rate of the transformed (product) phase is constant. This assumption has important consequences for the results of those models. Here, however, we extend the standard BNG model for cement hydration to incorporate time-dependence of the driving force for (and, therefore, rate of) C−S−H growth indicated by HydratiCA. The generalized BNG model still provides good fits to hydration rate data, albeit with different values of the fitting parameters; this indicates that the usual assumption of constant nucleation and growth rates is likely to result in erroneous values and interpretation of fitting parameters.

Finally, both HydratiCA and the generalized BNG model are used to draw conclusions about microstructure development in hydrating C_3S pastes, and to assess the relative likelihood of several hypotheses proposed in the literature to explain (1) the origin of the period of slow reaction shortly after mixing C_3S with water, (2) the observed peak in hydration rate that separates the acceleration period from the deceleration period and (3) the insensitivity of hydration kinetics to water/cement mass ratio (w/c).

1.1. The slow reaction period

Two quite different hypotheses, discussed in detail in refs. [2, 10], have been proposed to describe the origin of the period of slow reaction shortly after mixing with water, sometimes called the induction period or dormant period for portland cement. One hypothesis is that the C_3S dissolution rate decreases abruptly after a small degree of reaction owing to a change in the mechanism of dissolution [4, 11, 12]. We will refer to this as the "etch pit" theory because it is sometimes described in terms of a transition from etch pit unwinding at high driving forces to step-flow dissolution at lower driving forces. The other theory proposes the formation of a protective metastable hydrate layer on the surface of cement that partially seals the cement particle and inhibits dissolution [13, 14].

1.2. The rate peak

The transition from accelerating rates to decelerating rates has been alternately explained in terms of (1) a transition from control by C−S−H growth to control by diffusion through a thickening product layer on the surface of cement grains [15–17]; (2) eventual reduction in the surface area of C−S−H by bridging and filling the available space between cement particles [15]; or (3) reduction of C−S−H surface area by the lateral impingement of C−S−H precipitates growing along the surface of a single grain [18]. To be plausible, both hypotheses (2) and (3) require that C−S−H growth is the rate-controlling process both before and after the peak hydration rate; hydration kinetics would be unaffected by C−S−H surface area if C_3S dissolution controlled the rate. Based on evidence

that the magnitude and timing of the peak rate is about the same in pastes as it is in suspensions with high water/cement ratio, Garrault *et al.* [19] concluded that (4) C_3S hydration is controlled by C−S−H growth during the acceleration period but may change to control by C_3S dissolution during the deceleration period, and then to diffusion control at significantly later times [20].

Hypotheses (1) and (4) require a transition from C−S−H growth control to diffusion control and C_3S dissolution control, respectively. Such a transition would generally imply a change in the apparent activation energy for the net process [21]. The most recent and accurate measurements of activation energy for C_3S hydration show no change in the activation energy, at least for many hours after the peak rate [22]. A near equality of the activation energies for C−S−H growth and C_3S dissolution would be a remarkable coincidence because the solids have such different structures and compositions.

Computer modeling of the 3D microstructure and chemistry changes during C_3S hydration offers the opportunity to quantify the influences of the driving forces for the various processes, as well as the individual process rates and their dependence on solution composition in a way that is difficult, if not impossible, to do experimentally. In that sense, the kind of computer modeling we describe can complement experimental observations and help gain further insight into the origins of these hydration phenomena.

2. Modeling

2.1. HydratiCA

HydratiCA is a kinetic cellular automaton for simulating 3D microstructure evolution in aqueous suspensions by coupled transport and reactions. Stoichiometric solid phases (*e.g.*, $Ca(OH)_2$, C_3S), water, and aqueous solute species (*e.g.*, Ca^{2+}, OH^-) are defined as separate chemical components. Each material component is discretized into *cells*, each cell corresponding to a prescribed number of moles of that component. The initial microstructure of cement particles and water is mapped onto a cubic lattice by assigning cell occupations

numbers for each component at each site. Chemical and structural changes are simulated by iterating over small time steps during which independent reaction and transport processes occur. The probability, p_t, of a cell executing a random walk to a neighboring site is determined by that cell's local diffusivity, D, the time increment, Δt, and the lattice site spacing, λ:

$$p_t = \frac{D\Delta t}{\lambda^2} \tag{1}$$

Following the procedure developed by Karapiperis [23, 24], the probability of a unit reaction happening in a time step Δt depends on its rate constant and on the cell occupation number of each reactant. Equilibrium is established when the rates of the forward and reverse reactions become equal. The details of the algorithms and their validation are described elsewhere [2, 25].

HydratiCA can simulate multicomponent mass transport coupled with multiple heterogeneous or homogeneous reactions within 3D microstructures, but requires input of the various rate laws and rate constants, which in turn depends on accurate knowledge of the reaction mechanisms. Either the etch pit dissolution rates or the metastable barrier layer can be implemented in HydratiCA to simulate the slow reaction period by invoking alternate assumptions about the composition and physical properties of C−S−H. C−S−H is modeled as an intimate mixture of two stoichiometric compounds having Ca:Si molar ratios of 1:1 and 2:1. The main differences between the assumed metastable and stable forms of C−S−H are (1) metastable C−S−H forms on C_3S surfaces much as an adsorbed layer would, without requiring a nucleation step; (2) the compounds making up the metastable form each have solubility products that are about 100 times greater than their stable counterparts; and (3) the metastable forms are assumed to be about 1000 times more effective than their stable counterparts at restricting the access of C_3S to water. By adjusting within physically reasonable ranges the (currently) unknown thermodynamic and kinetic input data related to both C_3S and C−S−H, HydratiCA simulations can be made consistent with experimentally observed time dependence of the net hydration rate and pore

solution composition, as well as the dependence of Ca:Si molar ratio of C−S−H on the pore solution composition, regardless of whether the etch pit dissolution rates or the metastable barrier layer is used [2, 18, 25–28]. Therefore, HydratiCA cannot, by itself, assess the relative merits of these two theories based on comparisons to these kinds of experimental data. However, recent experimental measurements made by Nicoleau *et al.* [4] of the dependence of C_3S dissolution rate on undersaturation are consistent with the "etch pit" theory because they show a highly nonlinear dependence of the rate on the undersaturation in aqueous suspensions so dilute that formation of a metastable hydrate layer is improbable. The rate data obtained by Nicoleau are shown as discrete points in Fig. 1 as a function of the undersaturation, $\ln Q$, of the solution. Here we construct a least-squares regression to those data using an empirical rate law given by

$$\frac{dN_{\mathrm{C_3S}}}{dt} = -k_{\mathrm{C_3S}} A_{\mathrm{eff}} \left(1 - \exp\left[-\left(\frac{\ln K - \ln Q}{C_1}\right)^r\right]\right) \tag{2}$$

where $k_{\mathrm{C_3S}}$ is the dissolution rate constant at infinite dilution, approximated from the experimental data as $125.3\,\mathrm{\mu mol\,m^{-2}\,s^{-1}}$, A_{eff} is the C_3S surface area on which C−S−H growth can happen, which may be less than the actual C_3S surface area due to coverage by existing hydration product, and C_1 and r are constants determined by fitting Eq. (2) to the data by a least-squares method. The C_3S dissolution reaction assumed in ref. [4] is

$$\mathrm{C_3S + 5\,H_2O \rightleftharpoons 3\,Ca^{2+}_{(aq)} + H_4SiO_{4(aq)} + 6\,OH^-_{(aq)}} \qquad \ln K = -50.7 \tag{3}$$

where the *apparent* equilibrium constant given is the undersaturation at which the measured rate vanishes, which differs greatly from the true equilibrium constant for dissociation of anhydrous C_3S ($\ln K \sim 0$), possibly because of surface hydroxylation in water [4, 29]. The equilibrium constant for anhydrous C_3S appears to have little bearing on the kinetic behavior of dissolution, as demonstrated by Nicoleau et al. [4]. HydratiCA incorporates $H_3SiO_4^-$ and $H_2SiO_4^{2-}$,

but not H_4SiO_4, as the silicate components in solution. However, the reaction (3) can be transformed using the silicate speciation reaction [30],

$$H_4SiO_{4(aq)} + OH^-_{(aq)} \rightleftharpoons H_3SiO^-_{4(aq)} + H_2O \qquad \ln K = 9.6 \tag{4}$$

Adding the two reactions gives

$$C_3S + 5\,H_2O \rightleftharpoons 3\,Ca^{2+}_{(aq)} + H_3SiO^-_{4(aq)} + 5\,OH^-_{(aq)} \qquad \ln K = -41.1 \tag{5}$$

Reconciling the experimental measurements of C_3S dissolution rate plotted against $\ln Q$ to this new equation therefore involves only a horizontal shift along the abscissa by 9.6. The dimensionless parameters obtained by fitting Eq. (2) to the shifted experimental dissolution data are $C_1 = 21.05$ and $r = 3.73$. The quality of the fit is demonstrated in Fig. 1, in which the effective surface area fraction, A_{eff} is set to unity, and the activity product is defined by

$$Q = \{Ca^{2+}_{(aq)}\}^3\{H_3SiO^-_{4(aq)}\}\{OH^-_{(aq)}\}^5 \tag{6}$$

where we assume that the activity of water is unity, as justified by Raoult's law in solutions with ionic strengths as low as those simulated here. Nicoleau *et al.* also provided an empirical fit to their dissolution rate data using two functions fit to different ranges of $\ln Q$. We have chosen here to use the single function in Eq. (2), partly because it is easier to implement computationally, but more importantly because it converges to the net rate law required for an elementary reaction in the limit $C_1 \to 1$, $r \to 1$:

$$\frac{dC}{dt} = -ck\left(1 - \frac{Q}{K}\right) = -ck\,(1-\beta) \tag{7}$$

where C is the molar concentration of a reactant in an elementary reaction, c is the molar stoichiometric coefficient for that reactant, k is the absolute forward rate constant, and K is the equilibrium constant. The saturation index $\beta \equiv Q/K$ is defined so that $\beta > 1$ indicates supersaturation, $\beta = 1$ indicates equilibrium, and $\beta < 1$ indicates undersaturation with respect to the forward

reaction. Therefore, the same general form as Eq. (2) can embrace a wide range of rate behavior.

The effective C_3S surface area at a lattice site is defined in HydratiCA as

$$\frac{A_{\text{eff}}}{A} = 1 - \eta \min\left(1, \frac{\phi_{\text{CSH}}}{\phi_{\text{max}}}\right)^{2/3} \tag{8}$$

where A is the physical surface area of C_3S, η is the "opacity" of the product layer that forms on the surface (a measure of how effectively a unit area of coverage can inhibit dissolution), ϕ_{CSH} is the volume fraction of the lattice site occupied by C−S−H, and ϕ_{max} is the site volume fraction at which the surface is considered to be completely covered with a layer having opacity η. Phases with a low contact angle on C_3S, or those that grow essentially in 2D along the surface, will have relatively lower values of ϕ_{max}. The use of A_{eff} is necessitated by the fact that any lattice-based model cannot resolve the microstructure on a scale smaller than a single lattice site, which for these simulations is 1 µm. As indicated schematically in Fig. 2, the product within a lattice site could be distributed in any of a number of ways; once the surface of the cement is coated with product, that layer might be impermeable ($\eta = 1$) or present no obstacle to dissolution ($\eta = 0$). These parameters can be varied to give a wide range of hydration kinetic behavior, as illustrated in Fig. 3. In the remainder of the simulations, C−S−H is the only phase that is assumed to grow on the surface of C_3S, and the assumed values for η and ϕ_{max}, given in Table 1, were chosen to provide reasonable fits to a wide range of experimental measurements of C_3S hydration rates and pore solution compositions reported in the literature [3, 18, 27, 28].

Nucleation rates of C−S−H and portlandite are assumed to follow classical nucleation theory, with C−S−H nucleating heterogeneously on the surface of the cement grain (*i.e.*, the substrate) and CH nucleating homogeneously in the pore solution. The rate of formation of C−S−H nuclei ($\text{m}^{-2}\,\text{s}^{-1}$) is given by [31]

$$I_{\text{het}} = \frac{n_S D}{a^2} \exp\left[-\frac{q}{\ln^2 \beta}\right] \tag{9}$$

where n_S is the number of formula units of the nucleating species in contact with the substrate (m^{-2}), D is the diffusivity of the nucleating species, a is the characteristic dimension of a formula unit, β is the saturation index, and

$$q = \frac{16\pi\gamma_{\mathrm{CL}}\Omega^2 f(\theta)}{3k_{\mathrm{B}}^3 T^3} \tag{10}$$

where γ_{CL} is the crystal-liquid interfacial energy, $\Omega \approx a^3$ is the volume of a formula unit of the nucleating phase, k_{B} is Boltzmann's constant, θ is the contact angle between the crystal and the substrate, and

$$f(\theta) = [2 + \cos(\theta)]\sin^4(\theta/2) \tag{11}$$

If the area of nucleating substrate per unit volume of the system is O_V^B, then $n_S \approx O_V^B/a^2 \approx O_V^B/\Omega^{2/3}$. The rate of formation of nuclei per unit area of substrate is

$$I_{\mathrm{het}}^B = \frac{I_{\mathrm{het}}}{O_V^B} = I_0^B \exp\left[-\frac{q}{\ln^2\beta}\right] \tag{12}$$

where $I_0^B = D/\Omega^{4/3}$. The C−S−H product that forms from hydration of cement and C_3S has the composition $C_{1.7}SH_4$, density of $2050\,\mathrm{kg\,m^{-3}}$ and molar volume of $111\,\mathrm{cm^3\,mol^{-1}}$ [32]. This composition comprises both solid C−S−H (with H/S molar ratio 2.1) and internal water-filled gel pores totalling about 31 % of the total volume. For the simulations, C−S−H end members are chosen to have the same water content: CSH(I) = CSH_4 and CSH(II) = C_2SH_4. The molar volumes of these end members can be calculated by adding or subtracting the appropriate amount of CaO with molar volume of $16.8\,\mathrm{cm^3\,mol^{-1}}$ from the real C−S−H phase with C/S = 1.7 [32], resulting in values of $99\,\mathrm{cm^3\,mol^{-1}}$ and $116\,\mathrm{cm^3\,mol^{-1}}$ for CSH(I) and CSH(II), respectively. Therefore, the formula unit volumes for CSH(I) and CSH(II) are $\Omega_{\mathrm{CSH(I)}} = 1.68 \times 10^{-28}\,\mathrm{m^3}$ and $\Omega_{\mathrm{CSH(II)}} = 1.92 \times 10^{-28}\,\mathrm{m^3}$. In the absence of direct measurement of the CSH-liquid interfacial free energy, we estimate it using the approximate relationship

based on solubility proposed by Söhnel [33]:

$$\gamma_{\mathrm{CL}} \ \left(\mathrm{mJ\,m^{-2}}\right) \approx -16 \log_{10}\left(c_{\mathrm{eq}}/c^{\circ}_{\mathrm{eq}}\right) + 42.2 \tag{13}$$

where c_{eq} is the equilibrium molar concentration ($\mathrm{mol\,L^{-1}}$) of formula units in solution and $c^{\circ}_{\mathrm{eq}} = 1\,\mathrm{mol\,L^{-1}}$. To find c_{eq}, we note that each formula unit of CSH(I) that dissolves liberates one ion each of Ca^{2+}, $H_3SiO_4^-$, and OH^-, so the solubility is related to the equilibrium constant by

$$K_{\mathrm{CSH(I)}} = \{\mathrm{Ca}^{2+}_{(\mathrm{aq})}\}\{\mathrm{H_3SiO}^{-}_{4(\mathrm{aq})}\}\{\mathrm{OH}^{-}_{(\mathrm{aq})}\} = \left(y_{\mathrm{Ca}}\, c_{\mathrm{eq,I}}\right)\left(y_{\mathrm{Si}}\, c_{\mathrm{eq,I}}\right)\left(y_{\mathrm{OH}}\, c_{\mathrm{eq,I}}\right) \tag{14}$$

where the quantities in braces are activities and the y's are activity coefficients. Given $K_{\mathrm{CSH(I)}} = 1.5 \times 10^{-10}$, and approximating the solution as ideal, we estimate $c_{\mathrm{eq,I}} \approx (K_{\mathrm{CSH(I)}})^{1/3} \approx 0.53\,\mathrm{mmol\,L^{-1}}$; if the extended Debye-Hückel theory is used to calculate the ion activity coefficients [30], we obtain an activity of 0.586. Using these values in Eq. (13), we estimate the interfacial energy of CSH(I) with the solution is $\gamma_{\mathrm{CL,I}} \approx 94.6\,\mathrm{mJ\,m^{-2}}$ or $93.9\,\mathrm{mJ\,m^{-2}}$, respectively. Each formula unit of CSH(II) that dissolves liberates two Ca^{2+} ions, one $H_3SiO_4^-$, and three OH^-, so the solubility is found from

$$\begin{aligned} K_{\mathrm{CSH(II)}} &= \{\mathrm{Ca}^{2+}_{(\mathrm{aq})}\}^2\{\mathrm{H_3SiO}^{-}_{4(\mathrm{aq})}\}\{\mathrm{OH}^{-}_{(\mathrm{aq})}\}^3 \\ &= \left(2y_{\mathrm{Ca}}\, c_{\mathrm{eq,II}}\right)^2\left(y_{\mathrm{Si}}\, c_{\mathrm{eq,II}}\right)\left(3y_{\mathrm{OH}}\, c_{\mathrm{eq,II}}\right)^3 \end{aligned} \tag{15}$$

Approximating the solution as ideal, we estimate $c_{\mathrm{eq,II}} \approx \left(K_{\mathrm{CSH(II)}}/108\right)^{1/6} \approx 1.45\,\mathrm{mmol\,L^{-1}}$; taking account of the activity coefficients, we obtain an activity of 1.87. Using these values in Eq. (13), we find that the interfacial energy of CSH(II) with the solution is $\gamma_{\mathrm{CL,II}} \approx 87.6\,\mathrm{mJ\,m^{-2}}$ or $85.9\,\mathrm{mJ\,m^{-2}}$, respectively. Table 2 gives the values used for these parameters for C−S−H nucleating on C_3S and for portlandite nucleating in solution.

2.2. Boundary Nucleation and Growth

Models of boundary nucleation and growth (BNG) use experimental data to fit the model parameters. Such fitting to individual systems provides excellent agreement with the early kinetics of hydration of C_3S and cement [7, 9, 34, 35], and also with the hydration of MgO [36]. However, there are reasons to doubt the significance of the parameters obtained. First, the models were originally intended to describe phase changes in metals [5], not the sort of dissolution/precipitation reactions of present interest, where the growth rates on the two sides of the cement-water interface may be different and the entire volume of the system may not transform to the new phase(s). Second, the process may involve the growth of a low-density form of C−S−H that loosely fills the space originally occupied by water, followed by in-filling of interstices from new nucleation sites [8, 37], and the statistical methods used to account for impingement of products may not be valid in such a case [38]. Third, the growth rate of the product is assumed to be constant in time, but (as indicated by the present simulations) the supersaturation driving growth is not necessarily constant. Fourth, the BNG model allows for only a single product, whereas the hydration of cement results in several product phases (C−S−H, CH, ettringite, and others). Nevertheless, least-squares fitting of a model curve to experimental hydration kinetics data has been used to determine the parameters in several versions of the BNG model based on quite different physical assumptions regarding the distribution of nuclei [5], isotropy of growth [39], and confinement of the products [6], and they all agree equally well with the experimental data [40]. Indeed, the parameters extracted from these diverse models yield very similar (but not necessarily correct) nucleation densities and growth rates. The validity of these parameters is compromised by the assumption of a constant rate of growth (*i.e.*, a constant rate of propagation normal to the solution-hydrate interface), which implies a constant supersaturation of C−S−H. The present simulations done with HydratiCA provide a quantitative, continuous prediction of how β_{CSH} varies with time, so we will investigate a modified version of the BNG theory that (1) incorporates this same time dependence of β_{CSH} as in-

put and (2) enables the growth rate to be a function of the supersaturation, $G(\beta_{\mathrm{CSH}})$.

Let us suppose that the precipitate forms as an ellipsoidal particle on the surface of the unhydrated cement grain, with growth rates G_1 and G_3 in the plane of the surface, and G_2 normal to the surface, and that each growth rate is linearly dependent on the supersaturation:

$$G_k(t) = G_{0k}\left(\beta_{\mathrm{CSH}}(t) - 1\right) , \qquad k = 1, 2, 3 \tag{16}$$

where the G_{0k} are constants. The semi-axes of an ellipsoidal precipitate then increase with time according to

$$R_k(t) = G_{0k} \int_0^t \left(\beta_{\mathrm{CSH}}(t') - 1\right) \, dt' \equiv G_{0k}\xi(t) \tag{17}$$

where we call $\xi(t)$ the effecive time, by analogy to the form of the BNG model that assumes constant growth rates, $R_k(t) = G_k t$. HydratiCA simulations indicate that there is a high burst of supersaturation in the first minutes of hydration that is expected to result in nucleation of C−S−H, after which β_{CSH} remains low enough so that little additional nucleation is expected [3, 31]. Therefore, it is reasonable to assume that growth occurs from a fixed number of sites per unit area of cement, N_S, in which case the volume fraction of the system occupied by hydrates is [39]

$$X(t) = 1 - \exp\left[-2k_G\,\xi(t)\left(1 - \frac{F_D\left(k_S\,\xi(t)\right)}{k_S\,\xi(t)}\right)\right] \tag{18}$$

where F_D is the Dawson function, defined by

$$F_D(x) = e^{-x^2} \int_0^x e^{y^2}\, dy \tag{19}$$

The constants are defined by

$$k_G = r_G\, O_V^B\, G_{02} , \qquad k_S = G_{02}\sqrt{\pi N_S\, g} \tag{20}$$

where $1/2 \leq r_G \leq 1$ depends on whether the hydration products grow only outward into the solution ($r_G = 1/2$) or symmetrically into the water and particle

($r_G = 1$), O_V^B is the surface area of C_3S per unit volume of the system, and $g = G_{01}G_{03}/G_{02}^2$ is a measure of the growth rate anisotropy of the precipitate. Eq. (18) differs from Eq. (38) of ref. [39] only in that $\xi(t)$ replaces t.

HydratiCA outputs the degree of hydration, α, which is the volume fraction of C_3S consumed in the reaction, whereas the BNG model finds the volume fraction of the system consisting of hydration products, X. These two quantities are related by $\alpha = BX$, where B is given by [39][3]

$$\frac{1}{B} = \left(\frac{\rho_C/\rho_H}{R_{wc}\rho_C/\rho_w + 1}\right)\left(\frac{c + 1/\rho_C - 1/\rho_w}{1/\rho_H - 1/\rho_w}\right) \tag{21}$$

where $\rho_C = 3150$, $\rho_w = 1000$, $\rho_H = 2070$ are the densities ($\mathrm{kg\,m^{-3}}$) of C_3S, water, and the ensemble of hydration products, respectively, $R_{wc} = 0.90$ is the w/c ratio used in the simulations, and $c = -7.04 \times 10^{-5}\,\mathrm{m^3\,kg^{-1}}$ is the chemical shrinkage per kilogram of C_3S consumed by hydration [41]. For hydration of C_3S, $B \approx 1.73$ is used to convert the degree of hydration found from HydratiCA into X for comparison to the BNG model.

3. Results

Fig. 4 shows images made by HydratiCA of the initial particle and hydration products at hydration times of 3.5 h (where the hydration rate is at its maximum) and 24 h. The C_3S particle is 80 % covered with C−S−H by 10 h, with a mean C−S−H thickness of 0.35 µm, and by 24 h the mean layer thickness is 0.57 µm.

Fig. 5 shows that the saturation indices for both end-members of the C−S−H family rise to high values in the first minutes of hydration, causing C−S−H to nucleate on C_3S shortly before the peak in the saturation curves. Throughout the process, C_3S remains undersaturated ($\beta_{C_3S} < 1$). Upon precipitation of calcium hydroxide (CH) about one hour later, the calcium concentration drops, causing C_3S to dissolve more rapidly and the supersaturation of C−S−H to

[3] Ref. [39] has a typographical error, where the ρ_w in the numerator was shown as ρ_H.

increase temporarily. The values of β shown in Fig. 5 are obtained by averaging concentrations over the entire volume of the solution, but there is little difference between the surface concentration and the volumetric average. That is, the diffusion barrier is low enough so that the transport rate does not result in a significant concentration gradient.

The effect of the product layer's opacity is illustrated in Fig. 6, using the parameters listed in Table 3. When the layer provides no obstacle to dissolution (zero opacity), the degree of hydration (α) increases linearly at a rate much higher than observed in experimental measurements of C_3S hydration by Nonat for dilute suspensions [28] and by Kondo and Ueda for pastes [27]. In contrast, when the opacity $\eta \to 1$, the dissolution rate is so low that growth of C−S−H consumes the supersaturation and β_{CSH} approaches unity. At this point, dissolution becomes the rate-controlling step and the hydration rate is much lower than experimental measurements [18, 27, 28]. Intermediate opacity (Moderate) leads to significant supersaturation of C−S−H ($\beta_{\mathrm{CSH}} \gg 1$) and to dissolution rates that have been shown [26] to agree reasonably well with the reported rates of C_3S hydration in dilute suspensions and pastes [18, 27].

The time dependence of the supersaturation of C−S−H is sensitive to the opacity of the C−S−H growing on the C_3S surface, and this in turn has a significant influence on the linear growth rate predicted by the generalized BNG model, as illustrated in Fig. 7. The effective time, $R_k/G_{0k} = \xi$, is highly nonlinear, especially for the case of very high opacity. Under condtions of Moderate opacity, Fig. 8(a) shows that the BNG model accurately fits the rate of reaction simulated by HydratiCA when the β-dependence of growth rate is included. In contrast, Fig. 8(b) shows that the usual assumption of constant growth rate provides good agreement only up to the peak. In the case of high opacity, coverage of C_3S by C−S−H strongly retards dissolution and therefore leads to a strong drop in the growth rate. Consequently, the assumption that G is constant results in an overestimation of the post-peak growth rate by the BNG fit. Based on this latter result, one might erroneously conclude that there is a change in growth mechanism, such as a transition to diffusion control, after the peak.

To see the influence of the assumed opacity on the rate behavior, Fig. 9 plots the same properties as Fig. 8(b) under conditions of zero opacity (Fig. 9(a)) and high opacity(Fig. 9b)). When the opacity is high, the BNG fit underestimates the peak rate and overestimates the later rate, as shown in Fig. 9(a); when the opacity is zero, the BNG fit is good up to the peak, but underestimates the subsequent rate. The post-peak overestimate of the reaction rate in Fig. 9(a) is the opposite of the discrepancy typically reported in the literature (*e.g.*, [7]), where the curve obtained by regression falls below the data. This implies that the true opacity of the product layer is not very high. An important feature of all of these regression analyses is that the peak is predicted without requiring premature impingement; instead, it results from the physical interference of the product with the rate of dissolution, which causes a drop in the driving force for growth of C−S−H.

The BNG theory indicates that the fractional surface coverage, Y, of hydration products on the C_3S particle is given by [39]

$$Y(t) = 1 - e^{-Y_e} = 1 - e^{-(k_S \xi(t))^2} \tag{22}$$

where Y_e is the extended surface area, ignoring overlap of the hydration products [39]. Using the same parameters as in Fig. 8, the degree of coverage is seen to reach about 50 % by the time of the peak in the hydration rate (4 h to 5 h), and 100 % within $\sim$ 24 h, as shown in Fig. 10.

4. Discussion

Simulations performed with HydratiCA reproduce the reported rates of C_3S hydration and the concentrations of ions in the solution when the opacity of the product layer is set at a moderate value (Moderate, in Table 3) [3, 26]. With these values, the C−S−H that forms on the C_3S surface reduces, but does not completely stifle, the dissolution of the C_3S underneath. Throughout the 25 h of the simulation, the solution remains undersaturated with respect

to C_3S, particularly following precipitation of calcium hydroxide, but remains supersaturated with respect to C−S−H.

Given the size of the particle (surface area 218 µm^2, volume 262 µm^3) and the volume of the system (1000 µm^3), the specific surface area is $O_V^B = 0.22\,\mu\text{m}^{-1}$. Using the parameters from the fit in Fig. 8(a), the growth rate in the vicinity of the rate peak is $G_2 \approx 0.014\,\mu\text{m}\,\text{h}^{-1}$ and the density of nuclei is about $N_S \approx 14.7\,\mu\text{m}^{-2}$; the values obtained in the HydratiCA simulation were $0.0125\,\mu\text{m}\,\text{h}^{-1}$ and $11.3\,\mu\text{m}^{-2}$, respectively. The fit based on a constant growth rate (Fig. 8(b)) yields the same growth rate ($0.0133\,\mu\text{m}\,\text{h}^{-1}$), but a much higher nucleation density ($155\,\mu\text{m}^{-2}$) to compensate for the faster growth that occurs at early times when the driving force is high. These growth rates are somewhat lower than the values ($0.07\,\mu\text{m}\,\text{h}^{-1}$ to $0.09\,\mu\text{m}\,\text{h}^{-1}$) obtained using BNG models in refs. [7, 37], where the higher driving forces at early ages were not taken into account.

Of the hypotheses proposed in the literature for the peak in hydration rate, a transition to diffusion control [17, 27] is rendered unlikely by the observation that the apparent activation energy is the same both well before and well after the rate peak [22]. In fact, the cement grains are only about 50 % covered at the time of the rate peak, as indicated by these simulations and by earlier experiments [20]. Therefore, it is implausible that diffusion can become rate controlling at such early times and cause the rate peak.

The hypothesis that the rate peak is caused by impingement of hydration products alone [7, 42], possibly involving a low-density form of C−S−H that later densifies [8, 40], is plausible only if C−S−H growth controls the rate. C−S−H growth control would imply that C_3S dissolution is nearly at equilibrium ($\beta_{C_3S} \approx 1$). In contrast, the present simulation results in Fig. 5 indicate that, not only is C_3S not near equilibrium at the rate peak, but it is becoming progressively further from equilibrium— and C−S−H progressively closer to equilibrium. The C_3S dissolution rate is decreasing after the rate peak, by definition, despite the fact that the thermodynamic driving force for its dissolution continues to increase. Therefore, the reduction in dissolution rate must

be due to a kinetic factor, namely an increase in the fraction of C_3S surface obscured from the solution by C−S−H. To maintain realistic concentrations and hydration rates, the C−S−H opacity must be in a range where $\beta_{\mathrm{CSH}} \gg 1$, so there is no transition to diffusion controlled kinetics.

The major difference between this explanation of the rate peak and prior hypotheses related to lateral impingement of C−S−H is that prior hypotheses considered lateral impingement to be the primary cause of the peak due to the attendant reduction in C−S−H surface area [8, 19, 20]. Our simulation results indicate that the primary cause is loss of C_3S surface area by the overgrowth of C−S−H precipitates on the surface; their lateral impingement is a geometric consequence of that overgrowth but is not the reason for the peak.

The BNG fits in Fig. 8 and Fig. 9 were obtained by adjusting the parameters k_G and k_S in Eq. (18). Evaluation of Eq. (22) indicates extensive lateral impingement by hydration products on the surfaces of the particles. Fig. 11 shows that the extended surface coverage, Y_e, becomes significantly greater than the actual surface coverage, Y, when overlap of product on the surface is taken into account. However, there is relatively little impingement of product regions growing on different particles, as indicated by the small difference between the curves for X and the extended volume fraction, X_e, where [39]

$$X = 1 - e^{-X_e} \tag{23}$$

As with previous hypotheses of the rate peak relating to diffusion control or lateral impingement of C−S−H on the cement grains, the simulations here also imply that the rate peak is caused by local phenomena occurring on individual cement particles, and therefore is consistent with a number of experimental observations:

- The measured rate passes through a peak even under conditions of high dilution, where interparticle bridging by C−S−H is impossible [43].
- Even in pastes made at normal w/c ratios, the rate peak occurs at a degree of reaction too low to allow extensive particle impingement, unless

the initial product has very low density.

- The w/c ratio of a paste, which affects the average separation between particles, has almost no effect on the early hydration kinetics [44].

It is worthwhile emphasizing that the simulations here indicate that the overall C_3S hydration rate is influenced both by the rate of CSH growth and by the rate of C_3S dissolution, and thus neither can be considered the sole rate-controlling process from the onset of acceleration until long after the rate peak. This has been alluded to previously by Garrault *et al.* [19], and has been demonstrated quantitatively and mechanistically here. C_3S can establish kinetic control only if C−S−H is near equilibrium at the peak, but Fig. 5 shows that $\beta_{\mathrm{CSH}} \approx 15$ at the rate peak. This conclusion is also consistent with the observation that the apparent activation energy is unchanged from the beginning of the acceleration period until at least many hours after the deceleration period has begun [20, 22]. Increasing the opacity can bring β_{CSH} down to near unity, but only long after the rate peak (see Fig. 6). Even then, the high opacity leads to BNG growth rates that at 10 h are already too low compared to the HydratiCA simulations, as shown in Fig. 9(b).

5. Conclusion

Simulations using HydratiCA indicate that when C_3S is hydrated in water, the solution remains undersaturated with respect to C_3S and supersaturated with respect to C−S−H, from within the first second of contact with water until well after the rate peak. The reaction is therefore not controlled exclusively by either dissolution or growth, which may account for the observed constancy of the activation energy throughout much of early-age hydration. The decrease in rate after the peak is associated with partial blocking of the C_3S surface caused by increasing coverage by moderately opaque C−S−H, which reduces dissolution rates and thereby reduces the supersaturation and growth rate of C−S−H.

The simulations indicate that if the surface became covered by an impermeable layer, the rate of reaction would drop so rapidly that a BNG model with a constant growth rate would significantly overestimate the post-peak reaction rate. This is the opposite of the type of discrepancy seen when BNG models are applied to cement hydration, so it is likely that the hydration layer is only moderately effective at blocking dissolution sites on C_3S surfaces. In fact, the simulated rate of reaction and concentrations of ions agree with experiment only if moderate opacity is used. Therefore, there is no indication of a transition to diffusion control of the rate of hydration.

If the dependence of the growth rate on the saturation index is taken into account, a BNG model can account for the shape of the reaction rate peak without requiring significant impingement of hydration product between cement particles, although there is extensive lateral impingement as the particle becomes covered with the hydration product. This result also explains how the hydration rate of pastes can be almost independent of the water/cement ratio, as observed experimentally, without requiring a transition to diffusion control.

Acknowledgments

GWS was supported in part by Federal Highway Administration Grant DTFH61-12-H-00003 and ARRA Grant 611-473300-60026039 PROJ0002228. JWB was supported in part by Federal Highway Administration Interagency Agreement DTFH61-13-X-30003. The information in this paper does not necessarily reflect the opinion or policy of the federal government and no official endorsement should be inferred.

References

[1] H. F. W. Taylor, Cement Chemistry, 2nd Edition, Thomas Telford, London, 1997.

[2] J. W. Bullard, E. Enjolras, W. L. George, S. G. Satterfield, J. E. Terrill, A parallel reaction-transport model applied to cement hydration and

microstructure development, Modell. Simul. Mater. Sci. Eng. 18 (2010) 025007, eRB G2009-1289, PubID 902976.

[3] J. W. Bullard, R. J. Flatt, New insights into the effect of calcium hydroxide precipitation on the kinetics of tricalcium silicate hydration, J. Am. Ceram. Soc. 93 (7) (2010) 1894–1903.

[4] L. Nicoleau, A. Nonat, D. Perrey, The di- and tricalcium silicate dissolutions, Cem. Concr. Res. 47 (2013) 14–30.

[5] J. W. Cahn, The kinetics of grain boundary nucleated reactions, Acta Metall. 4 (1956) 449–459.

[6] E. Villa, P. R. Rios, Transformation kinetics for surface and bulk nucleation, Acta Mater. 58 (2010) 2752–2768.

[7] J. J. Thomas, A new approach to modeling the nucleation and growth kinetics of tricalcium silicate hydration, J. Am. Ceram. Soc. 90 (10) (2008) 3282–3288.

[8] S. Bishnoi, K. L. Scrivener, Studying nucleation and growth kinetics of alite hydration using μic, Cem. Concr. Res. 39 (10) (2009) 849–860.

[9] J. Zhang, E. A. Weissinger, S. Peethamparan, G. W. Scherer, Early hydration and setting of oil well cement, Cem. Concr. Res. 40 (2010) 1023–1033.

[10] J. W. Bullard, H. M. Jennings, R. A. Livingston, A. Nonat, G. W. Scherer, J. S. Schweitzer, K. L. Scrivener, J. J. Thomas, Mechanisms of cement hydration, Cem. Concr. Res. 41 (12) (2011) 1208–1223.

[11] D. Damidot, A. Nonat, C_3S hydration in dilute and stirred suspensions: (I) study of the two kinetic steps, Adv. Cem. Res. 6 (21) (1994) 27–35.

[12] P. Juilland, E. Gallucci, R. J. Flatt, K. Scrivener, Dissolution theory applied to the induction period in alite hydration, Cem. Concr. Res. 40 (6) (2010) 831–844.

[13] H. N. Stein, J. M. Stevels, Influence of silica on the hydration of 3 CaO,SiO_2, J. Appl. Chem. 14 (1964) 338–346.

[14] H. M. Jennings, P. L. Pratt, An experimental argument for the existence of a protective membrane surrounding Portland cement during the induction period, Cem. Concr. Res. 9 (1979) 501–506.

[15] E. M. Gartner, J. M. Gaidis, Hydration mechanisms, I, in: J. Skalny (Ed.), Materials Science of Concrete, Vol. 1, American Ceramic Society, Westerville, OH, 1989, pp. 95–125.

[16] E. M. Gartner, J. F. Young, D. A. Damidot, I. Jawed, Hydration of Portland cement, in: J. Bensted, P. Barnes (Eds.), Structure and Performance of Cements, 2nd Edition, Spon Press, New York, 2002, pp. 57–113.

[17] J. J. Biernacki, T. Xie, An advanced single particle model for C_3S and alite hydration, J. Am. Ceram. Soc. 94 (7) (2011) 2037–2047.

[18] S. Garrault, A. Nonat, Hydrated layer formation on tricalcium and dicalcium silicate surfaces: Experimental study and numerical simulations, Langmuir 17 (2001) 8131–8138.

[19] S. Garrault, L. Nicoleau, A. Nonat, Tricalcium silicate hydration modelling and numerical simulations, in: A. Kumar, K. L. Scrivener (Eds.), Proceedings of CONMOD 2010, Lausanne, Switzerland, 2010, pp. 91–94.

[20] S. Garrault, T. Behr, A. Nonat, Formation of the C–S–H layer during early hydration of tricalcium silicate grains with different sizes, J. Phys. Chem. B 110 (2006) 270–275.

[21] L. S. Darken, R. W. Gurry, Physical Chemistry of Metals, Metallurgy and Metallurgical Engineering Series, McGraw-Hill, New York, 1953.

[22] J. J. Thomas, The instantaneous apparent activation energy of cement hydration measured using a novel calorimetry-based method, J. Am. Ceram. Soc. 95 (10) (2012) 3291–3296.

[23] T. Karapiperis, B. Blankleider, Cellular automaton model of reaction-transport processes, Physica D 78 (1994) 30–64.

[24] T. Karapiperis, Cellular automaton model of precipitation/dissolution coupled with solute transport, J. Stat. Phys. 81 (1/2) (1995) 165–180.

[25] J. W. Bullard, Approximate rate constants for nonideal diffusion and their application in a stochastic model, J. Phys. Chem. A 111 (11) (2007) 2084–2092, eRB G2006-1935.

[26] J. W. Bullard, A determination of hydration mechanisms for tricalcium silicate using a kinetic cellular automaton model, J. Am. Ceram. Soc. 91 (7) (2008) 2088–2097, eRB G2008-0142.

[27] R. Kondo, S. Ueda, Kinetics and mechanisms of the hydration of cements, in: Proceedings of the Fifth International Symposium on the Chemistry of Cement, Part II. Hydration of Cements, Vol. 2, 1968, pp. 203–212.

[28] S. Garrault-Gauffinet, A. Nonat, Experimental investigation of calcium silicate hydrate (C-S-H) nucleation, J. Cryst. Growth 200 (1999) 565–574.

[29] P. Barret, D. Ménétrier, D. Bertrandie, Mechanism of C_3S dissolution and problem of the congruency in the very initial period and later on, Cem. Concr. Res. 13 (1983) 728–738.

[30] J. W. Ball, D. K. Nordstrom, User's manual for WATEQ4F, with revised thermodynamic database and test cases for calculating speciation of major, trace, and redox elements in natural waters, Open-File Report 91-183, U.S. Geological Survey (April 2001).

[31] D. Turnbull, Formation of crystal nuclei in liquid metals, J. Appl. Phys. 21 (1950) 1022–1028.

[32] J. J. Thomas, H. M. Jennings, A. J. Allen, Relationships between composition and density of tobermorite, jennite, and nanoscale $CaO–SiO_2–H_2O$, J. Phys. Chem. C 114 (2010) 7594–7601.

[33] O. Söhnel, Electrolyte crystal–aqueous solution interfacial tensions from crystallization data, J. Cryst. Growth 57 (1982) 101–108.

[34] B. Y. Lee, K. E. Kurtis, Influence of TiO_2 nanoparticles on early C_3S hydration, J. Am. Ceram. Soc. 93 (10) (2010) 3399–3405.

[35] F. Ridi, E. Fratini, P. Luciani, F. Winnefeld, P. Baglioni, Tricalcium silicate hydration reaction in the presence of comb-shaped superplasticizers: Boundary nucleation and growth model applied to polymer-modified pastes, J. Phys. Chem. C 116 (2012) 10887–10895.

[36] J. J. Thomas, S. Musso, I. Prestini, Kinetics and activitation energy of magnesium hydroxide (MgO) hydration, J. Am. Ceram. Soc. 97 (2014) 275–282.

[37] J. J. Thomas, A. J. Allen, H. M. Jennings, Hydration kinetics and microstructure development of normal and $CaCl_2$-accelerated tricalcium silicate pastes, J. Phys. Chem. C 113 (46) (2009) 19836–19844.

[38] S. Bishnoi, Geometric limitations of nucleation and growth models: Revisiting the impingement assumption, Cem. Concr. Res. 46 (2013) 30–40.

[39] G. W. Scherer, J. Zhang, J. J. Thomas, Nucleation and growth models for hydration of cement, Cem. Concr. Res. 42 (2012) 982–993.

[40] G. W. Scherer, Models of confined growth, Cem. Concr. Res. 42 (2012) 1252–1260.

[41] D. P. Bentz, P. Lura, J. W. Roberts, Mixture proportioning for internal curing, Concrete International 27 (2) (2005) 35–40.

[42] E. Masoero, J. J. Thomas, H. M. Jennings, A reaction zone hypothesis for the effects of particle size and water-to-cement ratio on the early hydration kinetics of C_3S, J. Am. Ceram. Soc. 97 (2013) 1–9.

[43] D. Damidot, A. Nonat, P. Barret, Kinetics of tricalcium silicate hydration in diluted suspensions by microcalorimetric measurements, J. Am. Ceram. Soc. 73 (11) (1990) 3319–3322.

[44] D. M. Kirby, J. J. Biernacki, The effect of water-to-cement ratio on the hydration kinetics of tricalcium silicate cements: Testing the two-step hydration hypothesis, Cem. Concr. Res. 42 (2012) 1147–1156.

List of Tables

Table 1: Properties of material components used in the simulations.

Component	V_m/ 10^{-5} m^3/mol	M/ kg/mol	σ/σ_o [(a)]	D/ 10^{-9} m^2/s	η [(c)]	$\phi_{\max}$ [(c)]
H_2O	18.1	0.018 02	1.0			
C_3S	72.4	0.228 33	0.0			
CSH(I)	99.0	0.188 23	0.01		0.9	0.2
CSH(II)	116.0	0.244 30	0.05		0.5	1.0
$Ca(OH)_2$	33.1	0.074 09	0.0			
Ca^{2+}		0.040 08		0.79		
$CaOH^+$		0.057 09		0.71		
$H_2SiO_4^{2-}$		0.094 10		0.70		
$H_3SiO_4^-$		0.095 10		0.70		
OH^-		0.017 00		5.28		

[(a)] Relative conductivity, the conductivity of the materials divided by that in the bulk solution.
[(b)] Ion mobility at infinite dilution.
[(c)] See Eq. (8) for the meaning of these terms for coverage of C_3S.

Table 2: Stoichiometry and assumed parameters for simulated reactions.

Reaction	k_+/ µmol/(m^n s)[a]	$\ln K$	ΔH/ kJ/mol	I_0^B/ m^{-n}/s[a]	q/ K^3
$C_3S + 4\,H_2O \rightleftharpoons 3\,Ca^{2+} + H_3SiO_4^- + 5\,OH^-$	125.3	-41.10	-137		
$CSH(I) \rightleftharpoons Ca^{2+} + H_3SiO_4^- + OH^- + 4\,H_2O$	0.003	-22.62	20	1.1×10^{27}[b]	2.5×10^{10}[b]
$CSH(II) \rightleftharpoons 2\,Ca^{2+} + H_3SiO_4^- + 3\,OH^- + 3\,H_2O$	0.003	-34.54	20	7.3×10^{26}[b]	2.0×10^{10}[b]
$Ca(OH)_2 \rightleftharpoons Ca^{2+} + 2\,OH^-$	7.2	-11.97	-17	4.0×10^{36}[c]	2.5×10^{9}[c]
$CaOH^+ \rightleftharpoons Ca^+ + OH^-$	6×10^5	-2.81	-22		
$H_3SiO_4^- + OH^- \rightleftharpoons H_2SiO_4^{2-} + H_2O$	1.5×10^7	1.91	-22		

[a] $n = 2$ or 3 for heterogeneous or homogeneous processes, respectively.
[b] Heterogeneous nucleation on C_3S.
[c] Homogeneous nucleation in solution.

Table 3: Opacity parameters used in Fig. 6. See Eq. (8) for the meaning of the parameters in the last two columns.

Designation	C−S−H End-member	Opacity, η	$\phi_{\max}$
Zero	I	0	0
	II	0	0
Moderate	I	0.9	0.2
	II	0.5	1.0
High	I	0.999	0.1
	II	0.999	0.1

List of Figures

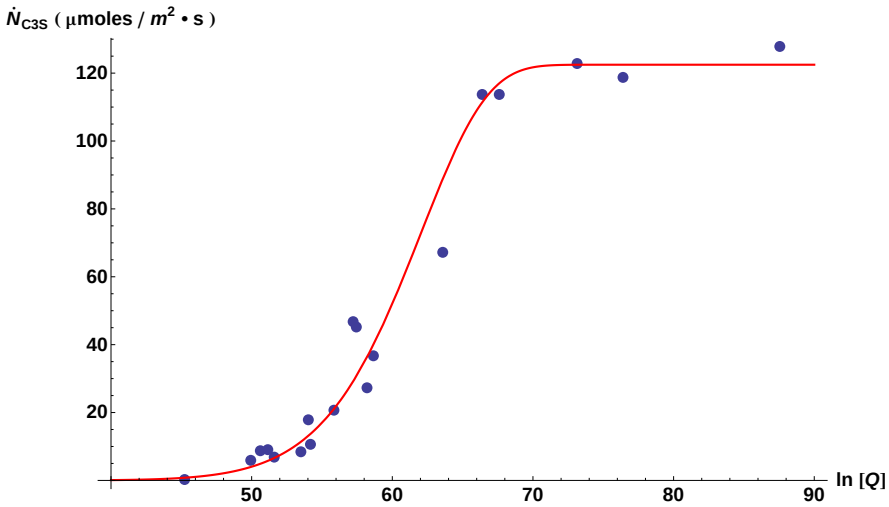

Figure 1: Dissolution rate of C_3S as a function of the activity product, Q defined in Eq. (6). The data points are from reference [4] and the curve was obtained by regression using Eq. (2).

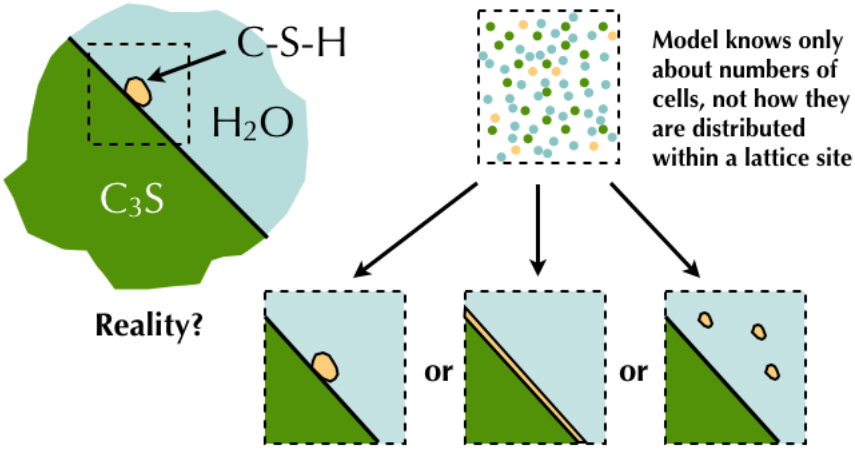

Figure 2: The volume of C–S–H at a lattice site in HydratiCA is known in terms of occupations numbers (*i.e.*, number of cells) at a site, but it could be distributed in any form within that site, including a single particle on the surface, a thin layer covering the surface, or multiple particles in the adjacent solutions.

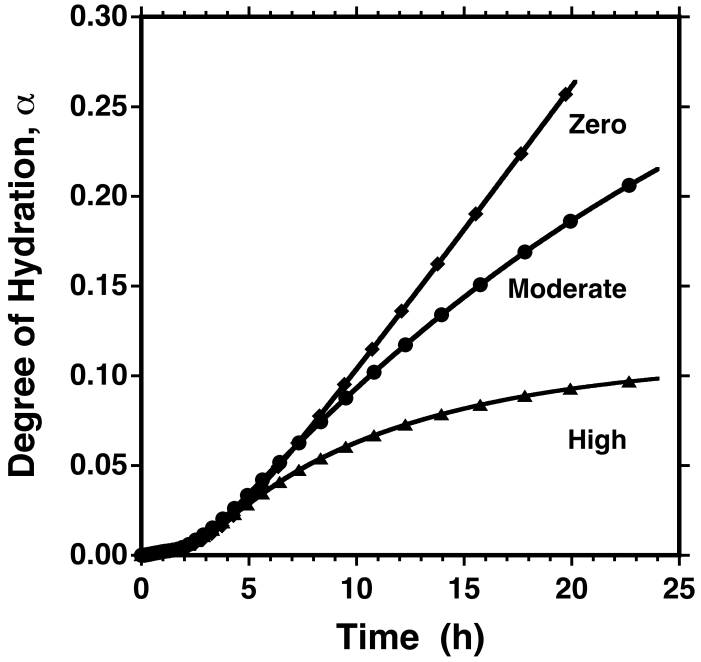

Figure 3: Influence of C–S–H opacity (*i.e.*, ability to suppress C_3S dissolution) on the progress of hydration with time.

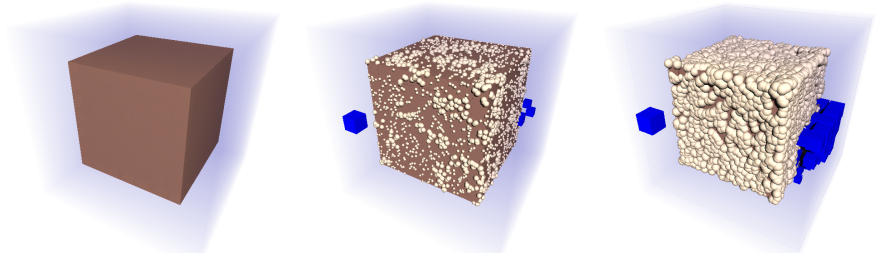

(a) (b) (c)

Figure 4: Microstructure of the hydration products on a single cubic particle of C_3S at (a) start of HydratiCA simulation, (b) 3.5 h of hydration, corresponding to maximum hydration rate, and (c) 24 h of hydration. C_3S (brown), C–S–H (beige), and CH (blue). Aqueous solution is shown as a light blue cloud filling the computational domain.

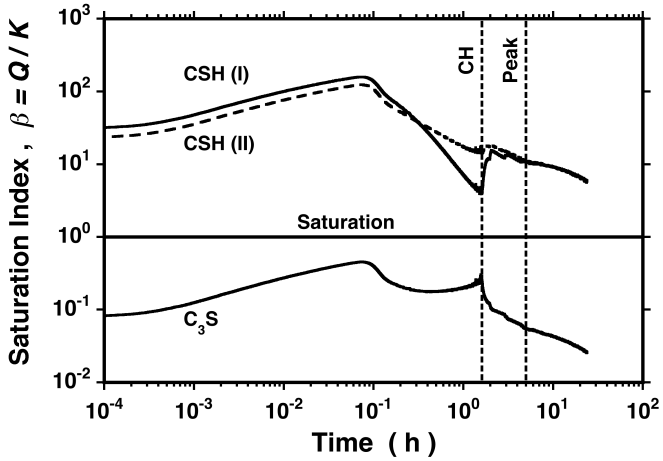

Figure 5: Results from HydratiCA simulations of C_3S hydration using Moderate opacity, showing saturation indices versus time after contact with water for the two end-member forms of C–S–H and for C_3S. Results are averaged over the whole volume of the solution. Vertical dashed lines indicate the times at which calcium hydroxide (CH) nucleates and the C–S–H precipitation rate passes through a maximum; the horizontal line at $\beta = 1$ indicates the equilibrium solubility for each phase.

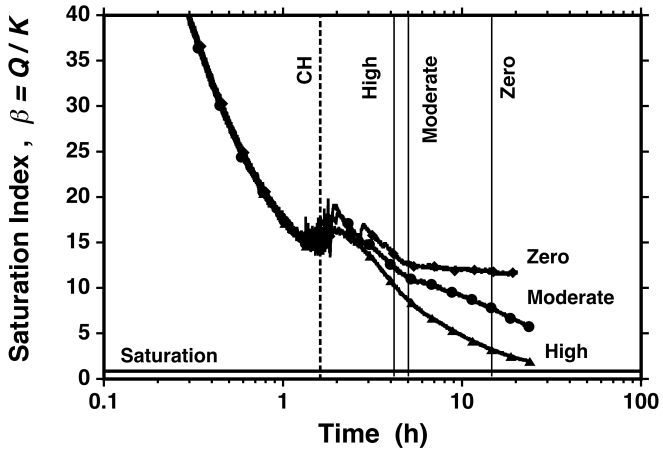

Figure 6: Saturation index of C–S–H versus time for three values of opacity (see Table 3). Vertical dashed line shows time of nucleation of calcium hydroxide (CH); thin vertical lines correspond to times of peak growth rate of C–S–H for High, Moderate, and Zero opacity (left to right); horizontal line indicates the equilibrium solubility ($\beta = 1$).

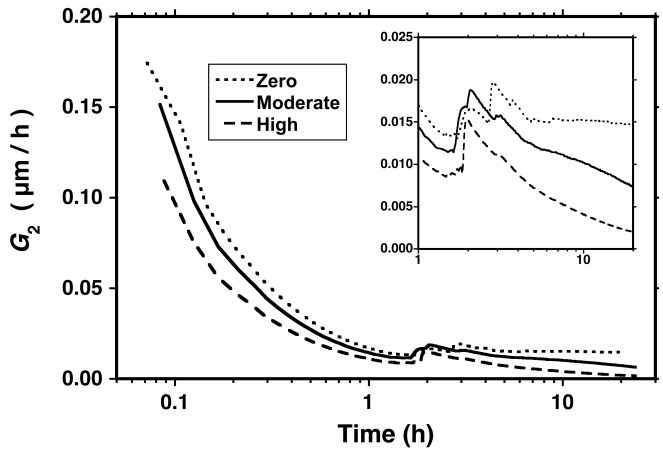

Figure 7: Growth rate found from Eq. (16) using the supersaturation given by HydratiCA (Fig. 5) with various values of opacity (see Table 3).

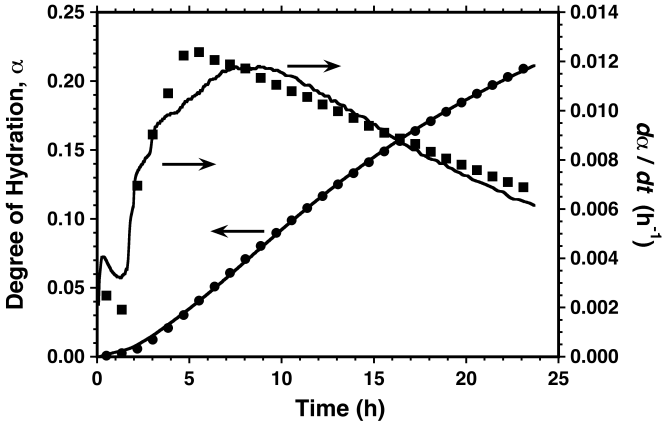

(a)

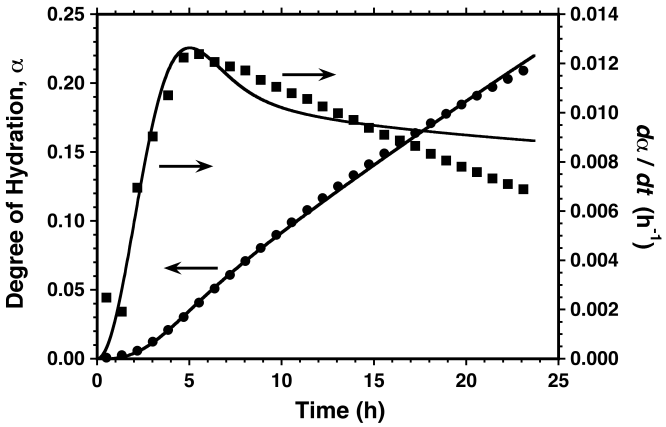

(b)

Figure 8: BNG approximation (solid curves) to HydratiCA simulations using Moderate opacity (black dots), assuming growth rate dependent on supersaturation (a) or a constant growth rate (b). Degree of hydration (DOH) is shown on the left ordinate and the rate of change of DOH is on the right ordinate. The BNG model is represented by Eq. (18) with ξ evaluated using β from HydratiCA.

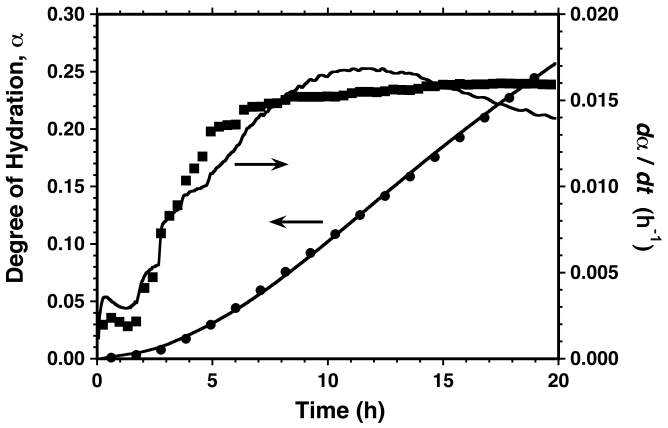

(a)

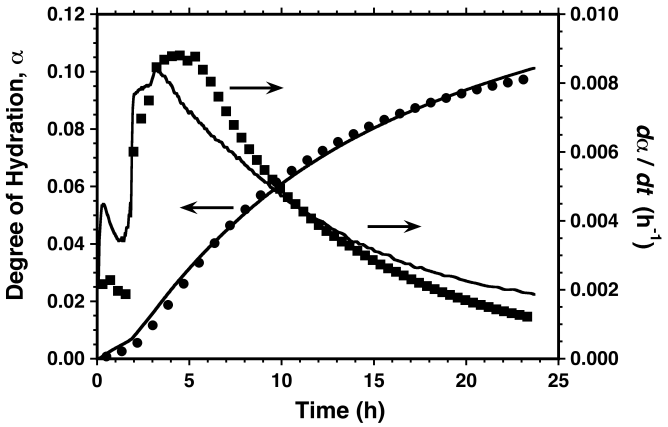

(b)

Figure 9: BNG approximation (solid curves) to HydratiCA simulations (black dots), assuming growth rate dependent on supersaturation, Zero opacity (a) or High opacity (b) (parameters from Table 3). Degree of hydration (DOH) is shown on the left ordinate and the rate of change of DOH is on the right ordinate. The BNG model is represented by Eq. (18) with ξ evaluated using β from HydratiCA.

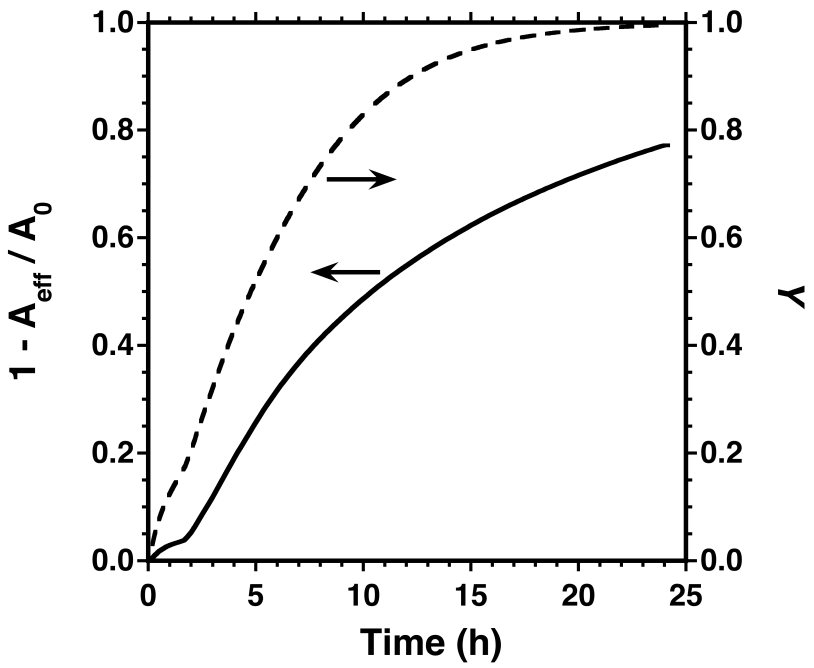

Figure 10: Fraction of the particle surface covered with hydration products according to HydratiCA with Moderate opacity (Solid)) and BNG (dashed).

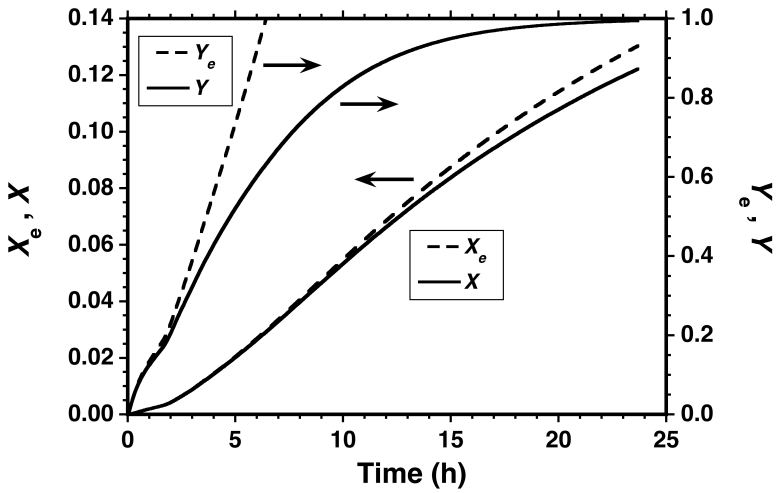

Figure 11: Extended volume fraction, X_e (dashed, left ordinate) and total volume fraction, X (solid, left ordinate), extended area fraction, Y_e (dashed, right ordinate) and total area fraction covered, Y (solid, right ordinate) found from BNG fit to HydratiCA data for Moderate opacity (Fig. 8(a).